

On the cool gaseous haloes of quasars

E. P. Farina^{1,2*}, R. Falomo³, R. Decarli⁴, A. Treves^{1,2,5}, and J. K. Kotilainen⁶

¹ *Università degli Studi dell'Insubria, via Valleggio 11, I-22100 Como, Italy*

² *INFN Milano-Bicocca – Università degli Studi di Milano-Bicocca, Piazza della Scienza 3, I-20126 Milano, Italy*

³ *INAF – Osservatorio Astronomico di Padova, Vicolo dell'Osservatorio 5, I-35122 Padova (PD), Italy*

⁴ *Max-Planck-Institut für Astronomie, Königstuhl 17, D-69117 Heidelberg, Germany*

⁵ *Associated to INAF*

⁶ *Finnish Centre for Astronomy with ESO (FINCA), University of Turku, Väisäläntie 20, FI-21500 Piikkiö, Finland*

ABSTRACT

We present optical spectroscopy of projected QSO pairs to investigate the Mg II and the CIV absorption features imprinted on the spectrum of the background object by the gaseous halo surrounding the foreground QSO. We observed 13 projected pairs in the redshift range $0.7 \lesssim z_F \lesssim 2.2$ spanning projected separations between 60 kpc and 120 kpc. In the spectra of the background QSOs, we identify Mg II intervening absorption systems associated to the foreground QSOs in 7 out of 10 pairs, and 1 absorption system out of 3 is found for CIV. The distribution of the equivalent width as a function of the impact parameter shows that, unlike the case of normal galaxies, some strong absorption systems ($EW_r > 1 \text{ \AA}$) are present also beyond a projected radius of ~ 70 kpc. If we take into account the mass of the galaxies as an additional parameter that influence the extent of the gaseous haloes, the distribution of the absorptions connected to the QSOs is consistent to that of galaxies. In the spectra of the foreground QSOs we do not detect any Mg II absorption lines originated by the gas surrounding the QSO itself, but in 2 cases these features are present for CIV. The comparison between the absorption features observed in the transverse direction and those along the line of sight allows us to comment on the distribution of the absorbing gas and on the emission properties of the QSOs.

Based on observations undertaken at the European Southern Observatory (ESO) Very Large Telescope (VLT) under Programmes 085.B-0210(A) and 086.B-0028(A).

Key words: galaxies: haloes — quasars: general — quasars: absorption lines

1 INTRODUCTION

Absorption lines in quasar (QSO) spectra provide a unique tool for probing the gas and dust content of foreground galaxies and of intergalactic medium at almost any redshift. Since the works of Bahcall & Spitzer (1969) and Boksenberg & Sargent (1978) these features are considered to be linked to large gaseous haloes around galaxies extending up to 100 kpc (see the review by Churchill, Kacprzak, & Steidel 2005). Despite a number of studies aimed at connecting metal absorption systems (in particular Mg II and CIV) with galaxy properties (e.g., Young, Sargent, & Boksenberg 1982; Lanzetta, Turnshek, & Wolfe 1987; Bergeron & Boissé 1991; Steidel & Sargent 1992; Steidel, Dickinson, & Persson 1994; Churchill et al. 1999; Rigby, Charlton, & Churchill 2002; Nestor, Turnshek, & Rao 2005;

Bergeron, Boissé, & Ménard 2011), the origin of the absorbing gas is still unclear. However, in the last decades, it is progressively emerging a scenario in which the stronger absorption lines (rest frame equivalent width $EW_r \gtrsim 1 \text{ \AA}$) are linked to winds driven by the star formation activity, while the weaker one are associated with inflows of gas onto the host galaxies.

For instance, Zibetti et al. (2007), stacking SDSS images of 2800 Mg II absorbers with $0.37 < z < 1.00$, show that the stronger absorption systems reside preferentially in blue star-forming galaxies, while the weaker ones in red passive galaxies. This result was confirmed by Ménard et al. (2011) in a sample of 8500 Mg II absorption systems present in the SDSS QSO spectra. They discovered a strong correlation between the EW_r of the absorbers and the luminosity of the associated [O II] lines, considered as a tracer of the star formation rate (SFR) of galaxies. Prochter, Prochaska, & Bures (2006) investigated the evolution of the number density of ~ 7400 Mg II strong absorption systems and found rough

* E-mail: emanuele.farina@mib.infn.it

correspondence with the evolution of the star formation rate at redshifts between $z = 0.5$ and 2, suggesting a link between the two phenomena. Recently Nestor et al. (2011) reported clear evidence that ultrastrong Mg II absorbers ($EW_r \gtrsim 3 \text{ \AA}$) reside in galaxies with very high SFRs. In addition to that, spectroscopic observations of highly star forming galaxies reveals the presence of blueshifted Mg II absorption features, further supporting the outflowing winds scenario (Tremonti, Moustakas, & Diamond-Stanic 2007; Weiner et al. 2009; Rubin et al. 2010; Martin et al. 2012).

The existence of a link between galaxy luminosity/halo mass and strength of absorption features, expected in the infalling scenario, is still debated. Chen, Lanzetta, & Webb (2001) and Chen et al. (2010a) found that the EW_r and the extent of Mg II and C IV absorption systems are related to host galaxy luminosity. More directly, Chen et al. (2010a) searched for absorption systems in a sample of 94 galaxies at redshifts between $z = 0.1$ and 0.5 within $pd \lesssim 85 \text{ kpc}$ from a QSO sightline. The EW_r of the systems found (the great majority of which have $EW_r \lesssim 1 \text{ \AA}$) scales with the stellar mass and only little with the star formation rate of the host galaxies (Chen et al. 2010b). These results are interpreted considering that Mg II absorption systems arise from infalling clouds to fuel star formation. Kacprzak et al. (2011) directly compared the relative Mg II halo gas and host galaxy kinematics for 13 L^* galaxies at $z \sim 0.1$. They found that these galaxies have low SFRs and a kinematically quiescent interstellar medium containing no outflowing gas. Given that these galaxies live in isolated environment, they suggest a scenario in which the cool gas halo was infalling and providing a gas reservoir that could maintain the low levels of star formation within the host galaxies. Bowen & Chelouche (2011), in a sample of Luminous Red Galaxies (LRGs) with redshifts $0.46 < z < 0.6$, found a low covering factor (k) for absorber with $EW_r \gtrsim 0.6 \text{ \AA}$ and a lack of correlation between EW_r and impact parameter or r-band absolute magnitude of the galaxies. They suggested that this is due or to the rich environment of these objects that makes their haloes too hot to maintain cool gas, or to the low rates of star formation that are not intense enough to fill their haloes with Mg II clouds. Cross correlating Mg II absorption systems and the properties of LRGs Bouché et al. (2006) found at redshift $z \sim 0.5$ an anti-correlation between the halo mass and the EW_r of absorbers (most of which have $EW_r \gtrsim 1 \text{ \AA}$), which suggests that the Mg II absorption systems are not virialised within the haloes. These results were further confirmed in larger sample by Lundgren et al. (2009) and by Gauthier, Chen, & Tinker (2009). Intriguingly, Rubin et al. (2012) detect inflow of gas into isolated star-forming galaxies at $z \sim 0.5$.

In contrast to the large attention given to absorptions detected around normal galaxies, only few studies have been focused on the properties of the gaseous halo of galaxies hosting a QSO in their centre. The observation of projected QSO pairs allows to probe the properties of the foreground QSO (QSO_F , $z \equiv z_F$), through the study of absorption features imprinted on the background QSO spectra (QSO_B , $z \equiv z_B > z_F$). The standard model on the origin of QSO high luminosity requires an intense gas accretion on a supermassive black hole that dramatically increases its activity. Feasible mechanisms responsible for the gas infall are in-

stabilities caused by strong gravitational interactions and galaxy mergers (e.g., Canalizo et al. 2007; Bennert et al. 2008; Green et al. 2010). The close (few hundreds kiloparsecs) environment of QSOs is expected to be populated by tidal debris, streams, and diffuse cool gas clouds, as commonly observed in interacting galaxies (e.g., Sulentic et al. 2001; Cortese et al. 2006). Given their low surface brightness, most of the properties of these features could be investigated almost exclusively in absorption, especially at high redshift.

Some studies have been performed to analyse the distribution of neutral hydrogen around QSOs. For instance Hennawi et al. (2006), starting from a sample of 149 projected QSO pairs (projected distance: $30 \text{ kpc} \lesssim pd \lesssim 2.5 \text{ Mpc}$; redshift: $1.8 < z_F < 4.0$), found that the probability to have an absorber with $N_{HI} > 10^{19} \text{ cm}^{-2}$ coincident within 200 kpc with a QSO_F is high ($\sim 50\%$), and that the distribution of these absorbers is highly anisotropic (Hennawi & Prochaska 2007, see also Kirkman & Tytler 2008; Prochaska & Hennawi 2009). The study of projected QSO pairs gives also the possibility to investigate the so-called *transverse proximity effect*: i.e., the expected decrease of absorption systems in the Ly α forest of a QSO_B due to the ionising flux of a QSO_F . Intriguingly the many attempts to measure this effect, with perhaps one exception (Gallerani et al. 2008), have led to only marginal or no detection (e.g., Crofts 1989; Dobrzycki & Bechtold 1991; Liske & Williger 2001; Schirber, Miralda-Escudé, & McDonald 2004). The presence of a transverse proximity effect for heavier elements is still unclear. For instance it was observed for He II by Worseck & Wisotzki (2006), but not for Mg II (Bowen et al. 2006) or for C IV (Tytler et al. 2009).

Up to now, only a few metal absorption systems associated or near to a QSO have been serendipitously discovered (e.g., Shaver, Boksenberg, & Robertson 1982; Shaver & Robertson 1983, 1985; Decarli, Treves, & Falomo 2009). The limited statistics is due to the little number of known close projected QSO pairs. Even the large spectroscopic QSO catalogue of the Sloan Digital Sky Survey, made of more than 100000 objects (Schneider et al. 2010), contains only 22 QSO pairs with separation less than $15''$. One should recall that the fiber collisions prevents the spectroscopic observations of two sources with separations below $55''$ in a single plate.

Tytler et al. (2009) studied the distribution of metal absorption features (in most case C IV) present in the spectra of 170 close ($z_B - z_F \lesssim 0.5$) projected QSO pairs with separations $100 \text{ kpc} \lesssim pd \lesssim 2.5 \text{ Mpc}$ in order to investigate their Mpc scale clustering properties around QSOs and other absorbers. They found 16 absorbers within $\pm 500 \text{ km/s}$ from the QSO_F , all with $pd > 400 \text{ kpc}$, that cluster with an approximately isotropic distribution, with a hint of an excess for systems with redshift $z < z_F$.

Bowen et al. (2006) select from the sample of projected QSO systems of Hennawi et al. (2006) 4 the pairs with $30 \lesssim pd \sim 100 \text{ kpc}$ and $0.5 \lesssim z_F \lesssim 1.5$. In all these systems they detect Mg II absorption lines clearly associated to QSO_F (see Figure 1). Despite the small sample size, they speculate that the absence of corresponding absorption lines in the spectra of QSO_F involve a non isotropic distribution of the absorbing gas. On the basis of these data

Chelouche et al. (2008) proposed that the gas in the outer region of QSOs (i.e., at radius larger than ~ 20 kpc) is distributed in the same way of L^* galaxies, but their thermal and ionisation structure is highly influenced by the central black hole emission.

In this paper we search for Mg II and CIV absorption features in a sample of 13 projected pairs. The aim of this work is to investigate the physical properties and the spatial distribution of the cool gas associated to the halo of QSOs. It is worth noting that the considered ions have very different ionisation energies, probing different gas conditions. The properties of the detected features are compared with those found in *normal* galaxies (i.e., galaxies not hosting a QSO) in order to investigate the effects of the central black hole emission on the cool gas.

We present our sample in §2 and the data reduction and analysis in §3. In §4 we investigate the properties of the detected absorption systems. In §5 we compare and contrast our results with those found in galaxies. We conclude and summarise in §6.

Throughout this paper we consider a concordance cosmology with $H_0 = 70$ km/s/Mpc, $\Omega_m = 0.3$, and $\Omega_\Lambda = 0.7$.

2 THE SAMPLE

We searched in the Véron-Cetty & Véron (2010) quasar catalogue for projected pairs that match the following requirements: (i) the angular separation is $\Delta\theta \lesssim 15''$ that, at the redshifts considered in our sample (i.e., $0.7 \lesssim z_F \lesssim 2.2$), allows us to explore the outer regions of a typical galaxy halo (i.e., from 60 to 120 kpc); (ii) the redshifts of fore- and background QSOs combine so that the CIV and Mg II emissions of the QSO_F fall within the wavelength range observed with FORS2 GRISM 1400V or GRISM 1200R, avoiding important sky features or narrow emission lines in the spectrum of the QSO_B; (iii) targets have declination $< 15^\circ$, so that they are visible from the Paranal site; and finally (iv) the QSO_B is brighter than $m_V \sim 21$ in order to collect spectra with signal-to-noise $S/N \gtrsim 10$. The resulting sample consists of 19 close pairs, 13 of which were observed with FORS2 at VLT.

In Table 1 and in Figure 1 we present the general properties of the 13 observed pairs. These are radio quiet QSOs, with an average angular separation of $11.4''$ that corresponds to an average projected distance of ~ 90 kpc. In our sample we do not take into account the presence of absorption *a priori*, thus it seems suitable to estimate the unbiased frequency of absorption systems.

3 OBSERVATIONS AND DATA ANALYSIS

3.1 Observations and data reduction

Spectra of the projected QSO pairs were collected with the VLT Antu telescope at the ESO Paranal observatory. Observations were performed with GRISM 1200R and 1400V on the FOCal Reducer/low dispersion Spectrograph (FORS2, see Appenzeller et al. 1998), yielding a spectral resolution of $R(1200R)=2900$ and $R(1400V)=2800$ (with the $1''$ slit). Typical exposure times are ~ 4000 seconds (~ 6000 seconds for fainter objects). The only exceptions are QQ08 and

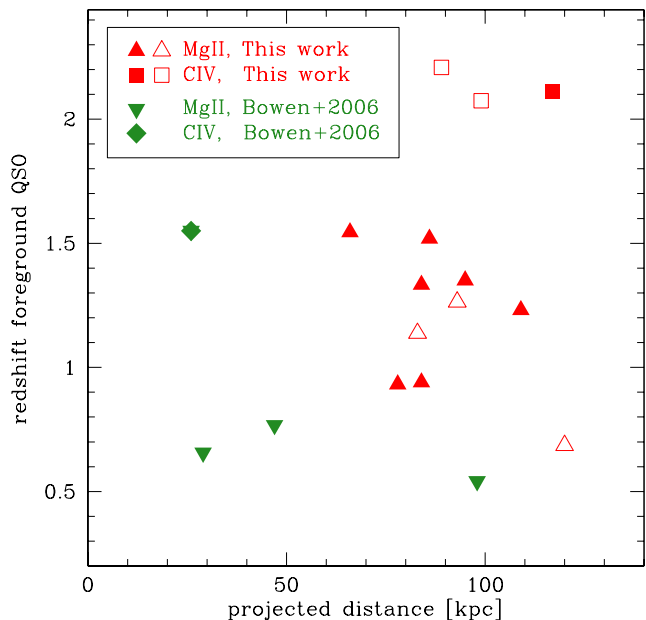


Figure 1. Distribution of close projected pairs in the $pd-z_F$ plane. Triangles are objects in which we investigate for the Mg II absorption features, while squares are for the CIV. The systems showing an absorption feature in the QSO_B spectra associated to the QSO_F are marked with filled points, otherwise with empty ones. Red and green points are from our sample and from that of Bowen et al. (2006), respectively. The systems discovered by (Tytler et al. 2009) have projected separations larger than 400 kpc and thus are not included in this Figure.

QQ09, for which exposures no longer than 2600 seconds were allowed by poor weather conditions.

Standard IRAF¹ tools were used in the data reduction. The `ccdred` package was employed to perform bias subtraction, flat field correction, image alignment and combination. Cosmic rays were eliminated by combining different exposures and by applying the `crreject` algorithm. The spectra extraction, the background subtraction, and the calibrations both in wavelength and in flux were performed with the `twodspec` and `onedspec` packages. Our accuracy in the wavelength calibration is $\sim 0.1 \text{ \AA}$. Galactic extinction was accounted for according to Schlegel, Finkbeiner, & Davis (1998), assuming $R_V = 3.1$. The spectra obtained are presented in Figure 2.

3.2 Analysis of the QSO Spectra

For the analysis of the QSOs spectra we followed the procedure presented in Decarli et al. (2010a) and De Rosa et al. (2011). Namely, data are first inspected by eyes and regions showing apparent absorption features are masked. Then, we designed the continuum with the superposition of: (i) the non thermal power-law-like component; (ii) the host galaxy star light (assuming the elliptical galaxy

¹ IRAF is distributed by the National Optical Astronomy Observatories, which are operated by the Association of Universities for Research in Astronomy, Inc., under cooperative agreement with the National Science Foundation.

Table 1. Properties of the observed QSO projected pairs: most common name of the foreground QSO, our identification label of the pair (ID), redshift from broad emission line (z_{bl}), absolute V -band magnitude of the QSO (V), angular ($\Delta\theta$) and projected (pd) separation, bolometric luminosity (L_{bol}), black hole mass (M_{BH} , see text for details), average seeing during observations (See.), and average signal-to-noise ratio per pixel on the continuum close to the expected position of the absorption lines (S/N , see §4). The label F and B refer to the foreground and to the background QSO, respectively. For notes on the individual objects see Appendix A.

QSO _F	ID	$z_{\text{bl,F}}$	$z_{\text{bl,B}}$	V_{F}	V_{B}	$\Delta\theta$ [arcsec]	pd [kpc]	$L_{\text{bol,F}}$ [10^{46} erg/s]	$M_{\text{BH,F}}$ [$\times 10^8 M_{\odot}$]	See. [arcsec]	S/N_{F}	S/N_{B}
SDSSJ00022-0053B	QQ01	1.542	2.205	-24.83	-26.66	7.8	66	0.89 ± 0.04	12.3	0.71	12	13
2QZJ003954-2725C	QQ02	1.262	2.100	-24.29	-23.96	11.1	93	0.56 ± 0.01	6.2	0.84	20	10
2QZJ004344-3000B	QQ03	1.346	1.554	-22.67	-24.71	11.3	95	0.27 ± 0.03	4.6	0.88	10	14
SDSSJ00541-0946B	QQ04	2.113	2.113	-25.59	-28.05	14.1	117	1.89 ± 0.02	13.7	1.41	49	20
Q0059-2702B	QQ05	0.941	1.963	-24.96	-23.95	10.7	84	2.23 ± 0.06	10.4	1.35	41	22
2QZJ011050-2719	QQ06	1.332	2.254	-23.59	-24.86	10.0	84	0.60 ± 0.02	6.8	1.36	23	10
2QZJ101636-0234A	QQ07	1.518	3.448	-25.65	-26.64	10.1	86	2.11 ± 0.13	9.9	0.75	15	15
2QZJ102425+0013A	QQ08	1.138	2.350	-23.99	-26.13	10.1	83	0.21 ± 0.05	0.9	1.18	6	9
SDSSJ11318-0222A	QQ09	2.198	2.353	-25.65	-26.95	10.8	89	0.54 ± 0.11	6.5	2.35	5	5
SDSSJ22028+1236A	QQ10	2.063	2.504	-26.80	-26.35	11.8	99	4.09 ± 0.11	24.4	0.89	31	16
SDSSJ22067-0039A	QQ11	1.230	1.516	-25.32	-25.60	13.1	109	1.41 ± 0.09	10.3	0.71	16	11
2QZJ222446-3200	QQ12	0.689	0.731	-23.32	-22.99	17.0	120	0.34 ± 0.03	1.3	0.79	29	18
Q2225-4023B	QQ13	0.931	2.398	-23.51	-26.24	9.9	78	0.26 ± 0.02	3.5	0.99	20	22

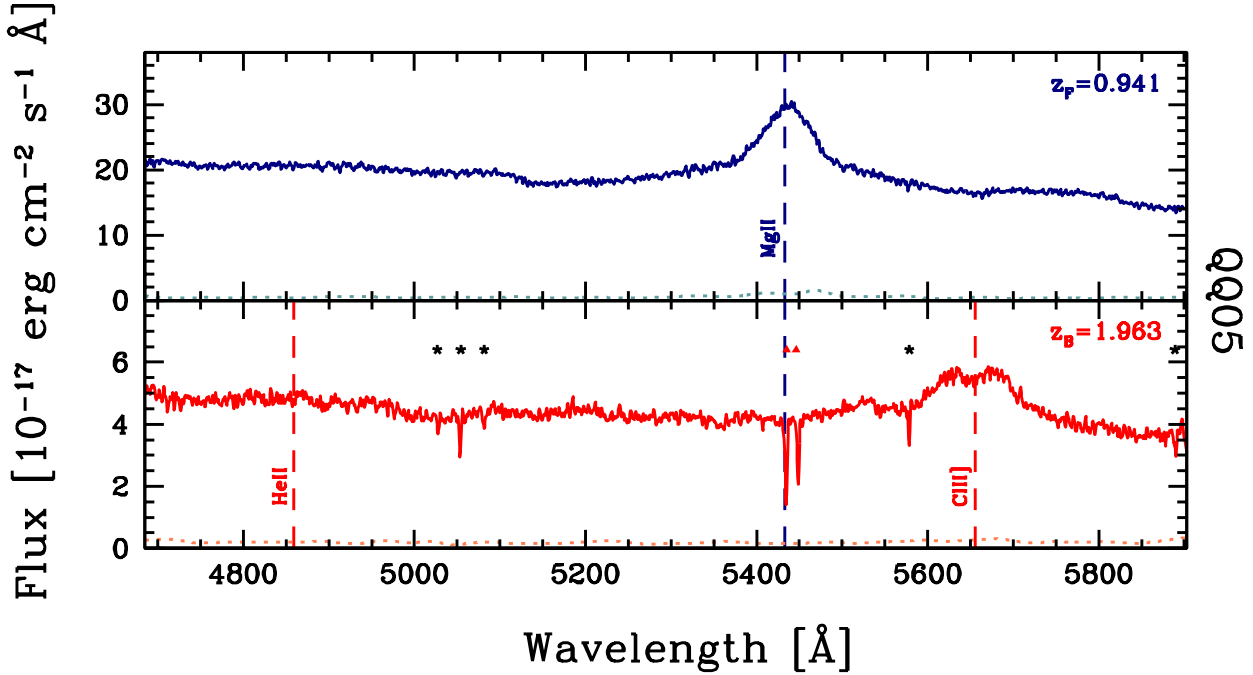


Figure 2. Spectra of the projected QSO pairs corrected for Galactic extinction. The blue solid lines refer to QSO_F and the red ones to QSO_B. The corresponding 1σ error spectrum is shown at the bottom of each panel. Triangles and squares point to all the Mg II and C IV absorptions identified, respectively, while stars to other lines detected above a 3σ threshold (see §3.3, Table 2 and Table A1). Main QSO emission lines are labelled and the gray regions mask regions with prominent telluric features. Figures for the remaining pairs are available only in the electronic edition of MNRAS.

template of Mannucci et al. 2001); and (iii) the contribution from blended Fe II multiplets (modelled with template of Vestergaard & Wilkes 2001 in the UV band and with our original spectrum of the narrow line Seyfert 1 galaxy I Zwicky 1 in the optical band). Finally, we have fitted broad emission lines with two Gaussian curves with the same central wavelength (see Decarli et al. 2008). Uncertainties on derived quantities are estimated from the 1σ errors in both continuum and line fits.

3.3 Analysis of the Absorption Features

Since the width of the absorption lines present in the spectra are smaller than the instrumental profile (FWHM ~ 100 km/s), for the analysis of the absorption features we considered a method similar to that adopted in the HST QSO Absorption Line Key Project (Schneider et al. 1993).

We split the spectrum of QSOs (after masking the apparent absorption features) in intervals of fixed size (20 Å, see for a similar approach Sbarufatti et al. 2005), and we modelled the “continuum” by interpolating the median values of the flux in each bin with a cubic spline function.

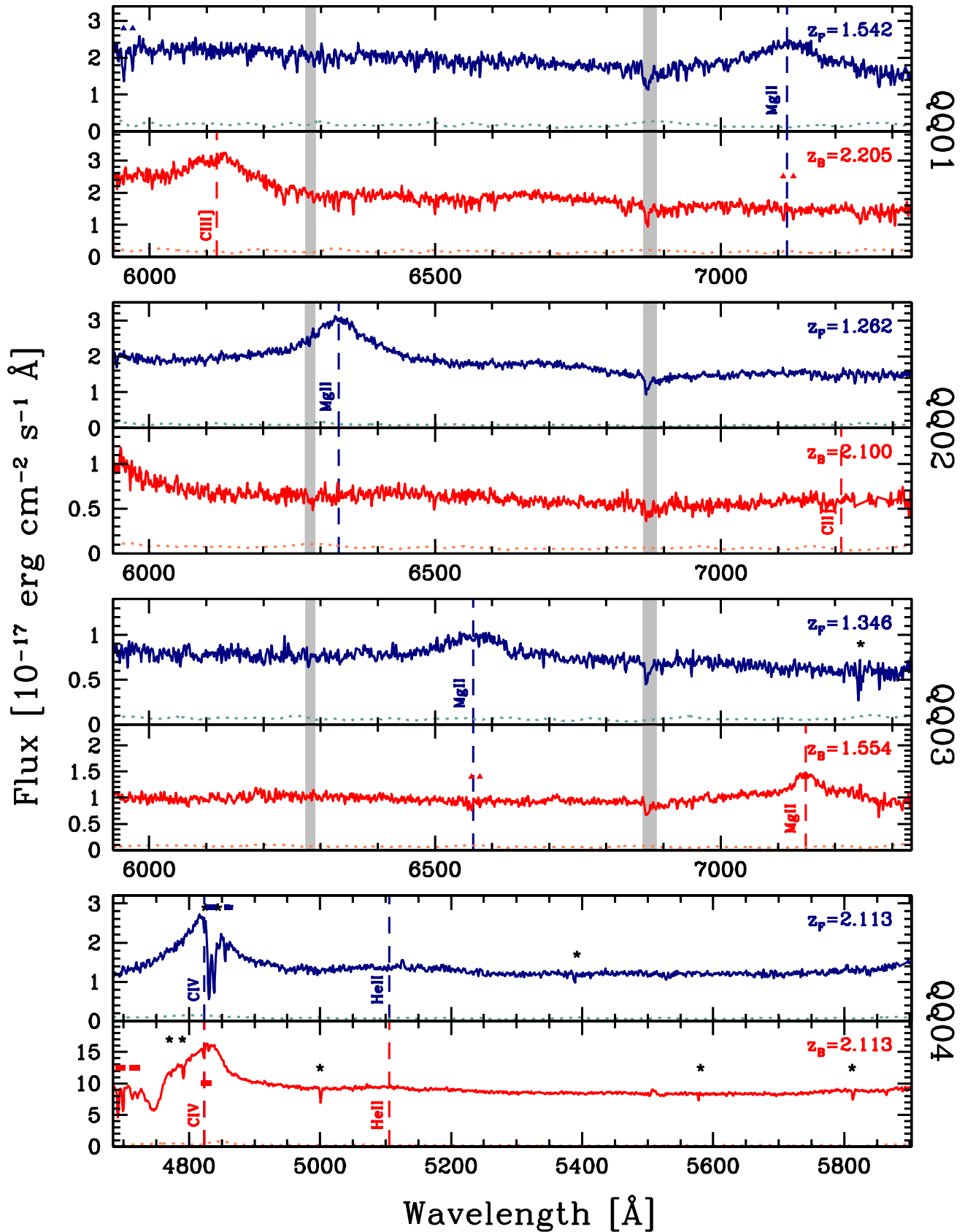


Figure 2. continued.

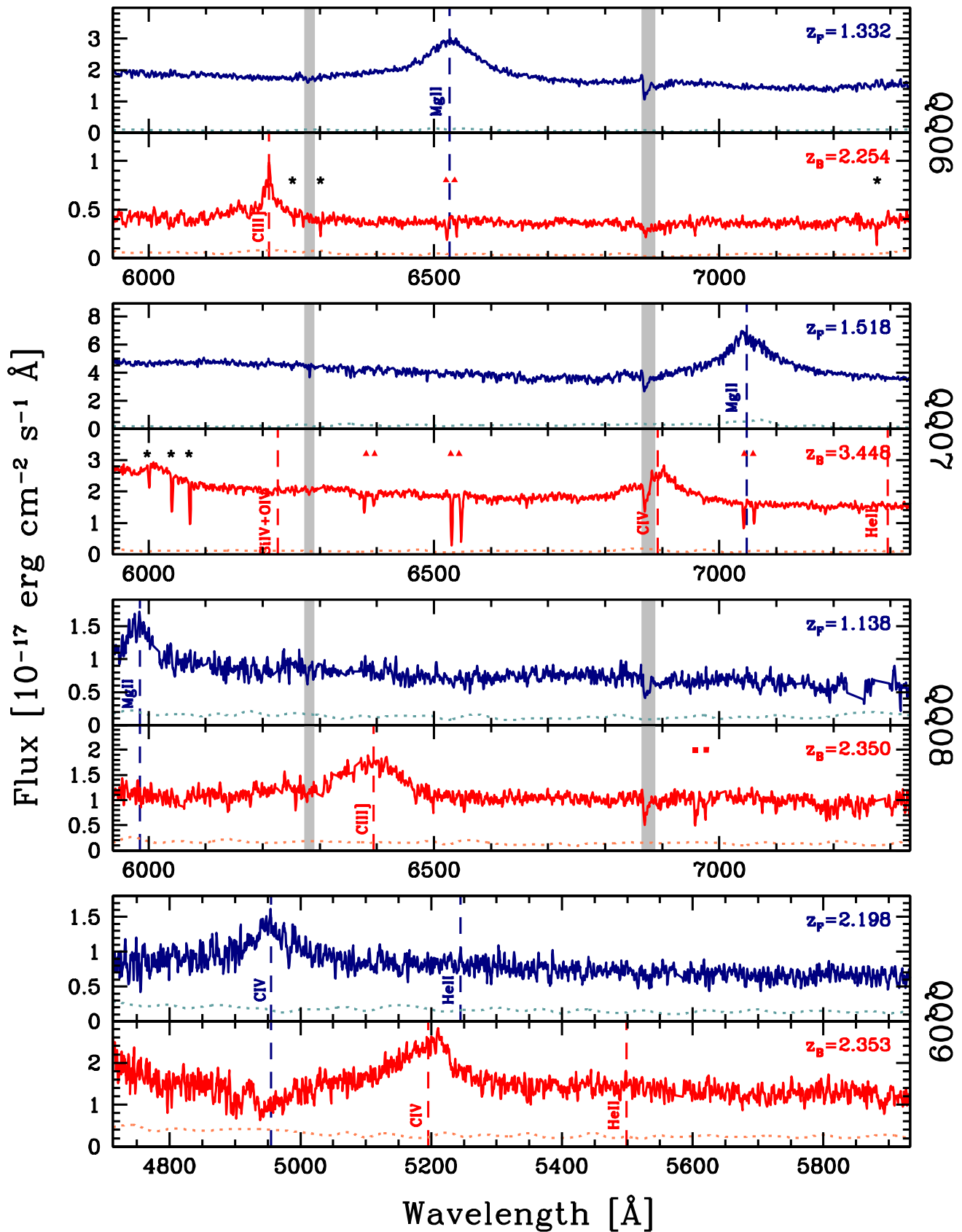


Figure 2. continued.

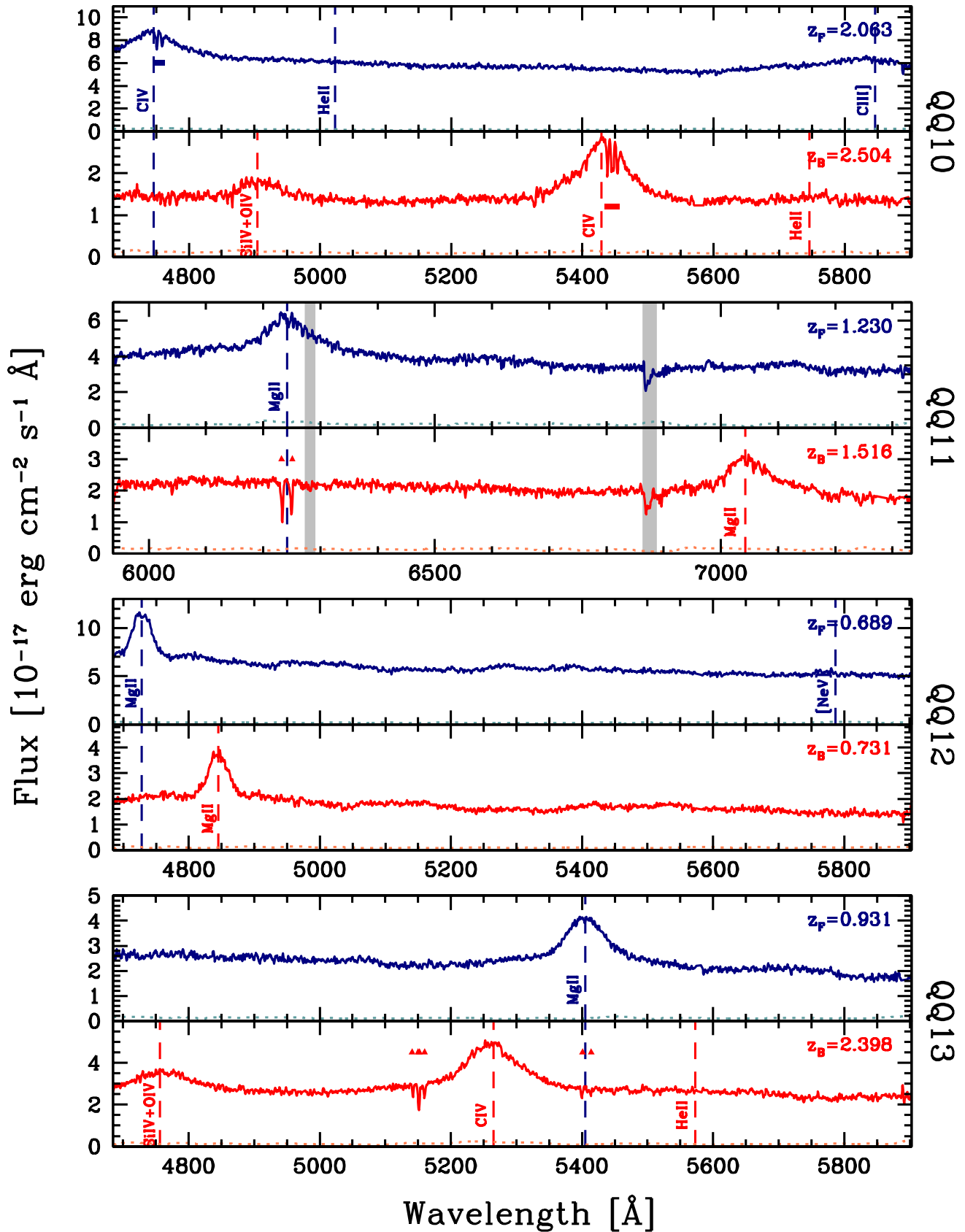


Figure 2. continued.

The equivalent width (EW) of an unresolved absorption feature and the relative uncertainties were calculated by modelling the Instrumental Spread Function (ISF) with a Gaussian with FWHM equal to the spectral resolution. From the redshift of the foreground QSOs, we are able to estimate the expected location of Mg II and CIV absorption features (see §4), thus a 3σ threshold imposed on the detection Mg II($\lambda 2796$) and CIV($\lambda 1548$) lines seems adequate to identify the absorption systems (e.g., Churchill et al. 2000).

The EWs and the centroid positions were measured by fitting a single Gaussian function (e.g., Churchill et al. 2000) on the detected absorption lines with our own software that performs a χ^2 minimisation procedure. The 1σ uncertainties were estimated through standard error propagation and assuming that largest source of errors is given by the continuum placement.

Figures 3 and 4 show the results of the fitting procedure on the detected absorption systems. Notes on the analysis of individual objects are in Appendix A.

4 ABSORPTION SYSTEMS ASSOCIATED TO QSOS

We estimate the covering factor (k) of cool gas around QSOs basing on the detection of absorbers close to the redshift of the QSO_F. It is well known that the redshifts derived from broad emission lines can differ from the systemic redshift by even hundreds km/s (e.g., Tytler & Fan 1992; Bonning, Shields, & Salviander 2007), and that absorbers within up to thousands km/s from a QSO are still connected with the QSO itself (e.g., Wild et al. 2008). Thus, as an operational definition, we consider an absorption system as associated to a QSO if its velocity difference with the the broad line redshift is smaller than ± 1000 km/s. Throughout the Paper, we will refer to *transverse* or to *line-of-sight* (LOS) absorption features associated to QSO_F depending on whether they are observed in the the spectrum of QSO_B or of QSO_F, respectively.

We can not discriminate between absorbers associated to the QSO_F and absorbers that occur by chance coincidence. However, the small separations in both projected distances and relative velocities suggest that we are probing the cool gas strictly related to the QSO.

The properties of the detected absorption systems associated to the QSO_F are listed in Table 2.

4.1 Transverse absorption systems

Mg II transverse absorption features are present in 7 out of 10 pairs (see Figure 3). Through the doublet ratio method (see e.g., Chan & Burbidge 1971; Falomo 1990), we can estimate an average column density of $\log(N_{\text{Mg II}}/\text{cm}^2) \sim 13.3$, assuming a Doppler parameter of $b \sim 5$ km/s (Churchill 1997).

Excluding QQ08, for which our data do not allow to state significant upper limit to EW_r , we estimated covering fraction of $k(\text{Mg II}) \sim 67\%$ for systems with $\text{EW}_r > 0.38 \text{ \AA}$. This value is lower than (but consistent within poissonian errors) the 100% found by Bowen et al. (2006) in a sample of 4 QSO pairs. Combining the two results we obtain $k(\text{Mg II}) \sim 77\%$ for $\text{EW}_r(\text{Mg II}) > 0.38 \text{ \AA}$. It is worth noting that, at higher

redshift, Hennawi et al. (2006) found a similar high covering fraction for HI absorbers ($k(\text{HI}) \sim 75\%$) in QSO pairs with projected separations $\text{pd} \lesssim 150$ kpc. Moreover, if we consider the empirical relation between the HI column densities and the Mg II equivalent widths estimated by Ménard & Chelouche (2009) in the sample of low-redshift Lyman absorbers of Rao, Turnshek, & Nestor (2006), we find that the covering fraction of $k(\text{HI}) = 50\%$ for absorbers with $\log(N_{\text{HI}}/\text{cm}^2) > 19$ calculated by Hennawi et al. (2006), exactly corresponds to the $k(\text{Mg II}) = 50\%$ for systems with $\text{EW}_r > 0.5 \text{ \AA}$ detected around low redshift QSOs.

The QSO Mg II covering factor seems to be larger than that observed in normal galaxies, although for these objects it spans a wide range of values, depending on impact parameter and galaxy properties: i.e., from $k(\text{Mg II}) \sim 10\%–15\%$ (Bowen & Chelouche 2011), to 25% (Bechtold & Ellingson 1992), to $\sim 50\%$ (Tripp & Bowen 2005; Kacprzak et al. 2008), up to $\sim 70\%$ (Chen et al. 2010a).

Only QQ04B shows a strong CIV absorption feature close to z_F (see Figure 3), formally yielding a covering factor of $k(\text{CIV}) \sim 30\%$. However, this feature is superimposed to the CIV broad emission lines of the QSO_B, and we can not exclude that it is instead a LOS absorption system associated to the QSO_B (see Appendix A). In the literature only few cases of CIV transverse absorption systems have been discovered, thus a sound value for the CIV covering factor around QSOs is still missing. Bowen et al. (2006) have detected a CIV absorption system in correspondence of a Mg II one in a QSO pair separated by a projected distance of 26 kpc. In their sample Tytler et al. (2009) found 16 CIV absorption features close in redshift to a QSO but both the small redshift difference and the large projected distance ($\text{pd} > 400$ kpc) of the QSO pairs they investigate do not allow to put constraints on the covering factor of CIV in the gaseous halo of the QSOs. Concerning galaxies, Chen, Lanzetta, & Webb (2001) have shown that at impact parameter $\lesssim 70$ kpc the CIV covering factor is nearly unity.

4.2 Line-of-Sight Absorption Systems

While no LOS absorption systems are observed for Mg II, these are present in 2 out of 3 of our spectra for CIV (in average $\log(N_{\text{CIV}}/\text{cm}^2) \sim 13.7$, assuming a Doppler parameter of 14 km/s D’Odorico et al. 1998, see Figure 4). This is in good agreement with Vanden Berk et al. (2008) and Shen & Ménard (2011a) who show that the occurrence of Mg II associated LOS absorption features in SDSS spectra is only of a few percent, and with Vestergaard (2003) that investigate a sample of moderate redshift QSO and found LOS narrow CIV absorption lines in $\gtrsim 50\%$ of them (see also, Wild et al. 2008). We stress that in general we can not discriminate between an origin of these absorbers close to the black hole, or in its host galaxy or in its surrounding halo (see for instance Crenshaw, Kraemer, & George 2003).

5 DISCUSSION

In Figure 5 we plot the rest frame equivalent width of Mg II transverse absorption systems against the QSO_F impact parameter. In spite of the small sample considered we note that many strong (i.e., $\text{EW}_r > 1 \text{ \AA}$) absorption systems are

Table 2. Properties of absorption features associated to the foreground QSO: our identification label of the QSO (ID), feature detected (Abs.), observed wavelength (λ_{abs}), rest frame equivalent width (EW_r), doublet ratio (DR), and redshift (z_{abs}). If no absorption system is present, the 2σ upper limit for the EW_r is quoted. The label F and B refer to absorption systems observed on the spectra of the foreground and of the background QSO, respectively.

Mg II						
ID	$\lambda_{\text{abs}}(\lambda 2796)$ [Å]	$\text{EW}_r(\lambda 2796)$ [Å]	$\lambda_{\text{abs}}(\lambda 2803)$ [Å]	$\text{EW}_r(\lambda 2803)$ [Å]	DR	z_{abs}
QQ01F	...	< 0.28	...	< 0.28
QQ01B	7109.0	0.48±0.17	7126.6	0.37±0.14	1.30±0.35	1.5421±0.0003
QQ02F	...	< 0.20	...	< 0.20
QQ02B	...	< 0.31	...	< 0.31
QQ03F	...	< 0.28	...	< 0.28
QQ03B	6564.1	0.46±0.12	6578.7	0.25±0.14	1.86±0.71	1.3470±0.0003
QQ05F	...	< 0.14	...	< 0.14
QQ05B	5434.5	1.21±0.09	5448.6	0.77±0.09	1.57±0.03	0.9434±0.0001
QQ06F	...	< 0.19	...	< 0.19
QQ06B	6522.8	0.91±0.17	6539.7	0.56±0.10	1.63±0.11	1.3326±0.0003
QQ07F	...	< 0.23	...	< 0.23
QQ07B	7043.0	0.58±0.07	7060.9	0.47±0.09	1.23±0.06	1.5186±0.0001
QQ08F	...	< 0.41	...	< 0.41
QQ08B	...	< 0.37	...	< 0.37
QQ11F	...	< 0.22	...	< 0.22
QQ11B	6233.4	1.36±0.16	6249.5	0.95±0.15	1.44±0.05	1.2291±0.0003
QQ12F	...	< 0.15	...	< 0.15
QQ12B	...	< 0.20	...	< 0.20
QQ13F	...	< 0.19	...	< 0.19
QQ13B	5399.6	0.24±0.07	5413.7	0.16±0.05	1.51±0.28	0.9310±0.0002
C IV						
ID	$\lambda_{\text{abs}}(\lambda 1548)$ [Å]	$\text{EW}_r(\lambda 1548)$ [Å]	$\lambda_{\text{abs}}(\lambda 1551)$ [Å]	$\text{EW}_r(\lambda 1551)$ [Å]	DR	z_{abs}
QQ04F	4830.3	1.42±0.12	4838.1	1.36±0.12	1.04±0.02	2.1198±0.0003
QQ04B	4822.4	0.12±0.02	4830.1	0.06±0.02	2.00±0.21	2.1147±0.0002
QQ09F	...	< 0.39	...	< 0.39
QQ09B	...	< 0.38	...	< 0.38
QQ10F	4751.3	0.14±0.03	4759.1	0.13±0.07	1.08±0.35	2.0689±0.0005
QQ10B	...	< 0.23	...	< 0.23

located up to separations larger than 70 kpc, in contrast to what observed in normal galaxies (see e.g., Chen et al. 2010a). In this Section we consider the host galaxy mass as an additional parameter that affects the EW_r -pd anti-correlation and we study how the QSO emission influence the distribution of the cool gas. In §5.3 we discuss possible origins of the absorbing gas.

5.1 The EW host galaxy mass relation

We here assume that all the Mg II absorption lines detected are associated to the gaseous halo of the QSOs. However, we can not exclude the possibility that some of these systems are due to intervening galaxies (see 5.3).

High resolution observations show that the Mg II ab-

sorbers associated to galaxies are often splitted in several discrete components (e.g., Churchill & Vogt 2001), suggesting a clumpy nature of the gaseous halo. Thus the EW_r of an absorption line is roughly proportional to the number of absorbing component along the line of sight (e.g., Petitjean & Bergeron 1990; Churchill, Vogt, & Charlton 2003).

For the sake of simplicity we here assume that the EW_r reflects the potential well of the dark matter halo and thus that the distribution of the cool gas around galaxies follow a spherical profile (e.g., Srianand & Khare 1993, 1994; Tinker & Chen 2008; Chelouche et al. 2008). At a given radius, the more massive systems sustain larger gaseous haloes that are responsible for stronger absorption lines due to the larger number of clouds intercepted. Assuming that the mass

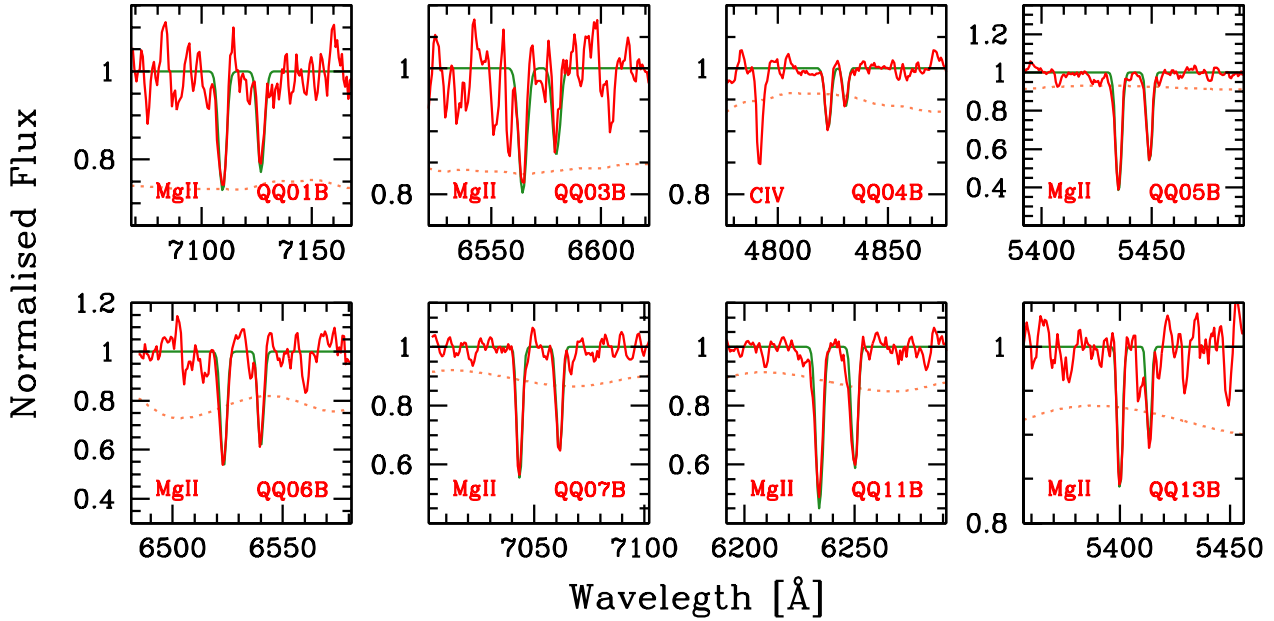


Figure 3. Close up of the normalised QSO_B spectra where the *transverse* absorption systems are detected (red line), the fit performed as described in §3 (green line), and the 3σ spectrum (pale red dotted line). The identification of the feature at ~ 4791 Å present in the spectra of QQ04B is uncertain due to the presence of the broad absorption line (see Appendix A). It seems not associated to any of the detected CIV absorption systems.

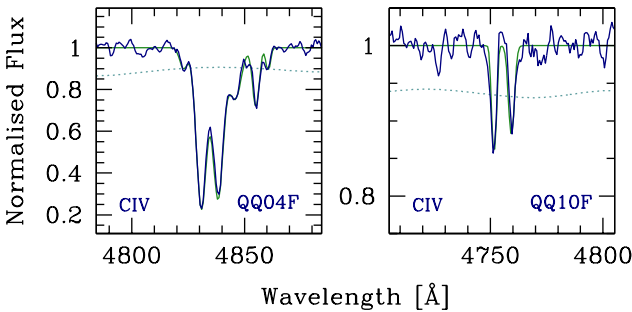


Figure 4. Close up of the normalised spectra of the QSOs QQ04F and QQ10F for which the associated LOS absorption features are detected (blue line), the fit performed as described in §3 (green line), and the 3σ spectrum (pale blue dotted line). For notes on the different CIV doublets superimposed to the broad emission line of QQ04F see Appendix A)

of the QSO host galaxy (M_{host}) trace the mass of the extend dark matter halo (see e.g., More et al. 2011), despite the uncertainties on the mass-to-light ratio, the EW_r of the absorption features is expected to follow a relation:

$$EW_r \propto \frac{M_{\text{host}}^\alpha}{pd^\beta}. \quad (1)$$

For instance, the two coefficients α and β have been estimated by Chen et al. (2010b) in a sample of low redshift galaxies ($z < 0.5$): $\alpha = 1.8 \pm 0.1$ and $\beta = 0.34 \pm 0.06$ (see Figure 6).

Is is worth of noting that the correlation between the EW_r and the mass of the halo is still not well established. For instance, Bouché et al. (2006), from an analysis of the relation between Mg II absorbers and luminous red galaxies in the SDSS found an anti-correlation be-

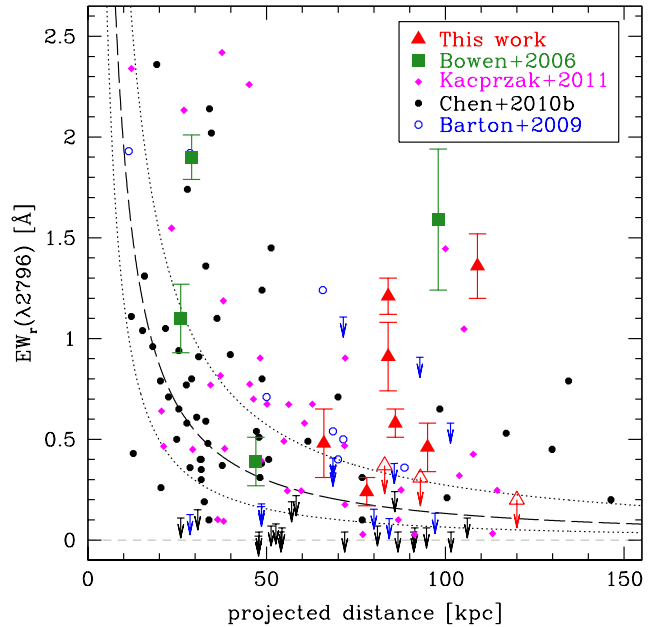


Figure 5. Rest frame EW_r of Mg II($\lambda 2796$) absorption line as a function of projected distance. Red filled triangle are the QSO_F in which this feature is detected and the empty ones are the 2σ upper limits. Green squares are data for QSOs from Bowen et al. (2006). Magenta diamonds, black filled points, and blue empty circles are absorption features associated to galaxies from Kacprzak et al. (2011), Chen et al. (2010a, also including the absorption detected in *group galaxies*), and Barton & Cooke (2009). For the sake of comparison, the upper limits listed by Barton & Cooke (2009) were converted to the considered 2σ limits. Black dashed line shows the best fit of the anti-correlation proposed by Chen et al. (2010a) and the associated 1σ uncertainties (dotted lines).

tween the absorber halo mass and EW_r , i.e., on average very strong absorbers ($EW_r \gtrsim 2 \text{ \AA}$) arise in less massive dark matter haloes ($\sim 10^{11} M_\odot$) while absorbers with $EW_r \sim 0.3 - 1.2 \text{ \AA}$ in the more massive one ($\sim 10^{12.5} M_\odot$). In addition Charlton & Churchill (1996) show that the Mg II distribution could be satisfactorily explained with both an extended disk geometry as well as a spherical one. From a sample of 40 galaxies at redshift ~ 0.5 , Kacprzak et al. (2011) suggest that the Mg II gas is distributed following a flattened halo that is co-planar and coupled to the inclination of the galaxy disc (see also, Kacprzak, Churchill, & Nielsen 2012).

In order to determine the mass of the host galaxy (M_{host}) of QSO_F we consider the $M_{\text{BH}}-M_{\text{host}}$ relation presented by Decarli et al. (2010b) that is based on the investigation of 96 QSOs with known host galaxy luminosities in the redshift range $0.07 < z < 2.74$:

$$\log \frac{M_{\text{BH}}}{M_{\text{host}}} = (0.28 \pm 0.06) z - (2.91 \pm 0.06) \quad (2)$$

where z is the QSO redshift. The M_{BH} s are estimated using the virial method applied to the gas of the BLR. These could be inferred from the width of broad emission lines and from the continuum luminosity, as expected from a photoionisation model (e.g., Kaspi et al. 2000). The uncertainties associated to the M_{BH} estimate are dominated by the dispersion of the relation between the radius of the BLR and the luminosity of the continuum and are typically around ~ 0.4 dex (e.g., Vestergaard & Peterson 2006; Shen et al. 2011b). The M_{BH} calculated from the recipes of Vestergaard & Peterson (2006) and of Vestergaard & Osmer (2009) are in Table 1.

In Figure 6 we show the distribution of the EW_r as a function of the impact parameter rescaled for the stellar mass for quiescent galaxies from Barton & Cooke (2009) and Chen et al. (2010b) (on average $M_{\text{gal}} \sim 10^{10} M_\odot$) and for the host of QSOs (on average $M_{\text{host}} \sim 2 \times 10^{11} M_\odot$). Taking into account the mass, the Mg II absorption systems associated to QSOs have a distribution close to that of galaxies. The value of the χ^2 for our data estimated on the relations presented by Chen et al. (2010a,b) prior and after accounting for the galaxy mass improves of a factor ~ 3 . This is in agreement with studies that suggest that the haloes of QSOs are similar to that of normal galaxies (e.g., Chelouche et al. 2008).

5.2 Effects of the QSO radiation

The presence of the intense radiation field coming from the central supermassive black hole should have a substantial effect in the thermal state of the gaseous halo. Chelouche et al. (2008) model the distribution of cool gas around QSOs suggesting that it is filled with clouds having size of ~ 1 pc and density of $\sim 10^{-2} \text{ cm}^{-3}$. Under these conditions a QSOs with luminosity of 10^{46} erg/s (the average of our sample calculated from the bolometric corrections given in Richards et al. 2006, see Table 1) can heat the cool gas within ~ 100 kpc up to a temperature of $T \sim 10^5$ K, allowing the existence of only few Mg II absorbers. Wild et al. (2008) from a sample Mg II absorber with equivalent width larger than 0.3 \AA directly associated to the QSOs, found that the QSO emission destroys Mg II clouds out to at least 800 kpc. Since the QSO radiation is thought to be emitted into cones

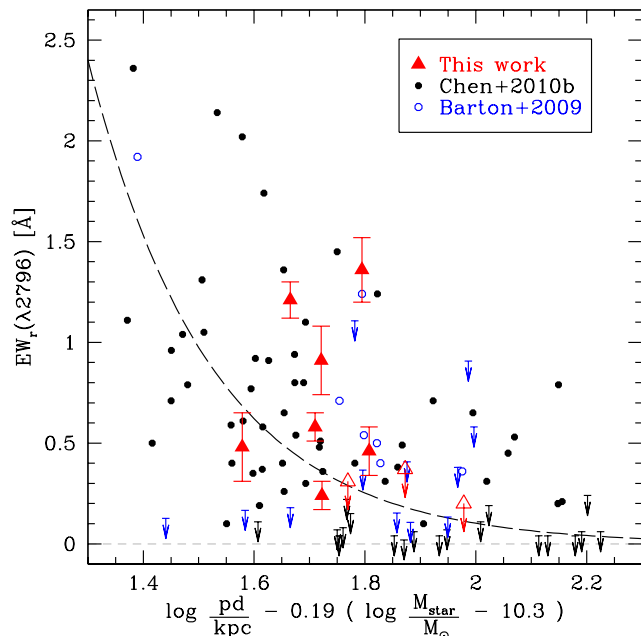


Figure 6. Rest frame EW_r of Mg II($\lambda 2796$) absorption line as a function of projected distance and stellar mass for QSOs and galaxies. Red filled triangles are systems for which the absorption system was detected, while the empty ones are 2σ upper limits. Empty blue and filled black circle are data for galaxies from Barton & Cooke (2009, with upper limits converted to the considered 2σ values) and Chen et al. (2010b), respectively. Black dashed line is the EW_r vs. projected distance anti-correlation for galaxies including the scaling relation with stellar mass proposed by Chen et al. (2010b). For the x-axis we have adopted the same projection of Figure 3 in Chen et al. (2010b).

(Antonucci 1993), an anisotropy of the distribution of absorbers is thus expected (e.g., Hennawi et al. 2006). If the UV emission of the central black occurs along the line of sight, the transverse absorption features will be not affected by it, and the QSO luminosity will have little impact on the extend Mg II absorbing gas at large galactic radii. On the contrary, Mg II absorbers along the line of sight are photoionised by the QSO emission (see also, Elvis 2000).

CIV and Mg II are believed to reside in the same halo clouds, however the ionising region of the former is expected to be smaller than that of the latter, consistent with its higher ionisation energy. CIV absorbers could survive within ~ 100 kpc, even though the radiation field of the QSO (Chelouche et al. 2008). The origin of the CIV LOS absorbers could also be associated to the region closer to the QSO. For instance, Wild et al. (2008), investigating the CIV LOS absorption system in a sample of ~ 7400 CIV absorbers from the SDSS, have found that $\sim 40\%$ of the systems within 3000 km/s of the QSO are due to a gas outflow from the central black hole (see also, Nestor, Turnshek, & Rao 2005).

5.3 Origin of Mg II absorbing gas

Although our sample of 13 QSO pairs does not allow us to put firm constraints, we can comment on the possible origin of the absorbing gas.

A simple explanation for the most intense and distant absorption lines detected around QSOs is that these are due to a chance superposition of a satellite galaxy or to the presence of tidal tail due to recent merger episodes (see e.g., Fumagalli et al. 2011; Keeney et al. 2011). This scenario is supported by studies suggesting that, despite the wide variety of environments in which they are detected, QSOs seem to prefer galactic environment richer than average (e.g., Wold et al. 2001; Serber et al. 2006; Hutchings, Scholz, & Bianchi 2009). However, the high covering factor and the observational evidence of galaxies surrounded by cool gas up to a radius of ~ 100 kpc, allow us to fairly assume the link between absorbers and QSO haloes. In support of this we also roughly estimate the the HI column density from the rest frame equivalent width of Mg II from the relations found in Ménard & Chelouche (2009). All the detected systems have $\log(N_{\text{HI}}/\text{cm}^2) < 19.6$, that is unlikely associated to galactic disc (e.g., Zwaan et al. 2005). However, we can not exclude the possibility that the absorptions origin from extra-planar neutral gas associated to spiral galaxies (e.g., Sancisi et al. 2008).

If the absorbers are associated to the QSO gaseous halos, the improvement of the anti-correlation between EW_r and projected distance due to the addition of the galaxy mass as parameter is naturally explained in the inflow scenario. As suggested by Chen et al. (2010b) more massive galaxies have more extended halos of cool gas and thus the observed Mg II absorbers arise in infalling clouds. However, we note that only the weaker absorption systems are thought to be associated to inflows of gas (the few absorption systems observed by Chen et al. at separations larger than 70 kpc have typically $\text{EW}_r \lesssim 0.7 \text{ \AA}$), while the stronger ones to outflows (e.g., Zibetti et al. 2007). The inflows of gas responsible of the QSO activity may produce intense star formation episodes and strong winds (e.g., Di Matteo, Springel, & Hernquist 2005; Hopkins et al. 2005; Maiolino et al. 2012) that might give rise to the stronger detected absorption lines. This is also supported by the recent discovery of signature of high star formation rate and gas outflows in the QSO host galaxies (Floyd et al. 2012; Sanmartim, Storch-Bergmann & Brotherton 2012).

6 SUMMARY AND CONCLUSIONS

We studied 13 close projected QSO pairs observed with FORS2 at ESO-VLT. The projected separations of the systems (between 60 kpc and 120 kpc) allowed us to investigate the presence of Mg II and C IV absorption systems in the outer regions of the extended gaseous haloes of QSOs in the redshift range $0.7 \lesssim z_F \lesssim 2.2$.

In 7 out of 10 systems we have detected the Mg II doublet on the QSO_B spectrum in correspondence to the QSO_F , while only one association out of 3 is found for C IV. We compare our results with those performed for normal galaxies by Kacprzak et al. (2011), Chen et al. (2010a), and Barton & Cooke (2009). If we consider EW_r as a function of both the projected distance and the mass of the systems, we find that the haloes of QSOs are similar to that of galaxies. In our small sample, we do not detect a significant enhancement of the absorption system strengths, as could be expected if the QSO nuclear activity were driven by intense

gas accretion onto the black hole. Finally, we note that along the line of sight we do not detect any Mg II absorbers of the same strength of the transverse one. These results are in agreement with models that consider a non isotropic emission of the QSO, which are hosted by gaseous haloes more massive than those of galaxies.

ACKNOWLEDGEMENTS

We acknowledge helpful discussions with C. Montuori, F. Haardt, and M. Fumagalli. For this work EPF was supported by Società Carlo Gavazzi S.p.A. and by Thales Alenia Space Italia SpA. RD acknowledges funding from Germany's national research centre for aeronautics and space (DLR, project FKZ 50 OR 1104). This work was based on observations made with the ESO/VLT Telescope in Paranal.

REFERENCES

- Antonucci R., 1993, *ARA&A*, 31, 473
 Appenzeller I., et al., 1998, *Msngr*, 94, 1
 Bahcall J. N., Spitzer L., Jr., 1969, *ApJ*, 156, L63
 Barton E. J., Cooke J., 2009, *AJ*, 138, 1817
 Bechtold J., Ellingson E., 1992, *ApJ*, 396, 20
 Bennert N., Canalizo G., Jungwiert B., Stockton A., Schweizer F., Peng C. Y., Lacy M., 2008, *ApJ*, 677, 846
 Bergeron J., Boissé P., 1991, *A&A*, 243, 344
 Bergeron J., Boissé P., Ménard B., 2011, *A&A*, 525, A51
 Bonning E. W., Shields G. A., Salviander S., 2007, *ApJ*, 666, L13
 Bowen D. V., et al., 2006, *ApJ*, 645, L105
 Bowen D. V., Chelouche D., 2011, *ApJ*, 727, 47
 Boksenberg A., Sargent W. L. W., 1978, *ApJ*, 220, 42
 Bouché N., Murphy M. T., Péroux C., Csabai I., Wild V., 2006, *MNRAS*, 371, 495
 Canalizo G., Bennert N., Jungwiert B., Stockton A., Schweizer F., Lacy M., Peng C., 2007, *ApJ*, 669, 801
 Chan Y. W. T., Burbidge E. M., 1971, *ApJ*, 167, 213
 Charlton J. C., Churchill C. W., 1996, *ApJ*, 465, 631
 Chelouche D., Ménard B., Bowen D. V., Gnat O., 2008, *ApJ*, 683, 55
 Chelouche D., Bowen D. V., 2010, *ApJ*, 722, 1821
 Chen H.-W., Lanzetta K. M., Webb J. K., 2001, *ApJ*, 556, 158
 Chen H.-W., Helsby J. E., Gauthier J.-R., Shethman S. A., Thompson I. B., Tinker J. L., 2010a, *ApJ*, 714, 1521
 Chen H.-W., Wild V., Tinker J. L., Gauthier J.-R., Helsby J. E., Shethman S. A., Thompson I. B., 2010b, *ApJ*, 724, L176
 Churchill C. W., 1997, *PhDT*
 Churchill C. W., Rigby J. R., Charlton J. C., Vogt S. S., 1999, *ApJS*, 120, 51
 Churchill C. W., Mellon R. R., Charlton J. C., Jannuzi B. T., Kirhakos S., Steidel C. C., Schneider D. P., 2000, *ApJS*, 130, 91
 Churchill C. W., Vogt S. S., 2001, *AJ*, 122, 679
 Churchill C. W., Vogt S. S., Charlton J. C., 2003, *AJ*, 125, 98
 Churchill C. W., Kacprzak G. G., Steidel C. C., 2005, *pgqa.conf*, 24

- Crenshaw D. M., Kraemer S. B., George I. M., 2003, *ARA&A*, 41, 117
- Cortese L., Gavazzi G., Boselli A., Franzetti P., Kennicutt R. C., O’Neil K., Sakai S., 2006, *A&A*, 453, 847
- Crotts A. P. S., 1989, *ApJ*, 336, 550
- Decarli R., Labita M., Treves A., Falomo R., 2008, *MNRAS*, 387, 1237
- Decarli R., Treves A., Falomo R., 2009, *MNRAS*, 396, L31
- Decarli R., Falomo R., Treves A., Kotilainen J. K., Labita M., Scarpa R., 2010a, *MNRAS*, 402, 2441
- Decarli R., Falomo R., Treves A., Labita M., Kotilainen J. K., Scarpa R., 2010b, *MNRAS*, 402, 2453
- De Rosa G., Decarli R., Walter F., Fan X., Jiang L., Kurk J., Pasquali A., Rix H. W., 2011, *ApJ*, 739, 56
- Dobrzycki A., Bechtold J., 1991, *ApJ*, 377, L69
- Di Matteo T., Springel V., Hernquist L., 2005, *Natur*, 433, 604
- D’Odorico V., Cristiani S., D’Odorico S., Fontana A., Gillalongo E., 1998, *A&AS*, 127, 217
- Elvis M., 2000, *ApJ*, 545, 63
- Farina E. P., Falomo R., Treves A., 2011, *MNRAS*, 415, 3163
- Falomo R., 1990, *ApJ*, 353, 114
- Floyd D. J. E., Dunlop J. S., Kukula M. J., Brown M. J. I., McLure R. J., Baum S. A., O’Dea C. P., 2012, *arXiv*, arXiv:1208.4143
- Fumagalli M., Prochaska J. X., Kasen D., Dekel A., Ceverino D., Primack J. R., 2011, *MNRAS*, 418, 1796
- Gallerani S., Ferrara A., Fan X., Choudhury T. R., 2008, *MNRAS*, 386, 359
- Gauthier J.-R., Chen H.-W., Tinker J. L., 2009, *ApJ*, 702, 50
- Green P. J., Myers A. D., Barkhouse W. A., Mulchaey J. S., Bennert V. N., Cox T. J., Aldcroft T. L., 2010, *ApJ*, 710, 1578
- Hennawi J. F., et al., 2006, *ApJ*, 651, 61
- Hennawi J. F., Prochaska J. X., 2007, *ApJ*, 655, 735
- Hewett P. C., Wild V., 2010, *MNRAS*, 405, 2302
- Hopkins P. F., Hernquist L., Cox T. J., Di Matteo T., Martini P., Robertson B., Springel V., 2005, *ApJ*, 630, 705
- Hutchings J. B., Scholz P., Bianchi L., 2009, *AJ*, 137, 3533
- Kaspi S., Smith P. S., Netzer H., Maoz D., Jannuzi B. T., Giveon U., 2000, *ApJ*, 533, 631
- Kacprzak G. G., Churchill C. W., Steidel C. C., Murphy M. T., 2008, *AJ*, 135, 922
- Kacprzak G. G., Churchill C. W., Evans J. L., Murphy M. T., Steidel C. C., 2011, *MNRAS*, 416, 3118
- Kacprzak G. G., Churchill C. W., Nielsen N. M., 2012, *arXiv*, arXiv:1205.0245
- Keeney B. A., Stocke J. T., Danforth C. W., Carilli C. L., 2011, *AJ*, 141, 66
- Kirkman D., Tytler D., 2008, *MNRAS*, 391, 1457
- Lanzetta K. M., Turnshek D. A., Wolfe A. M., 1987, *ApJ*, 322, 739
- Liske J., Williger G. M., 2001, *MNRAS*, 328, 653
- Lundgren B. F., et al., 2009, *ApJ*, 698, 819
- Maiolino R., et al., 2012, *MNRAS*, 425, L66
- Mannucci F., Basile F., Poggianti B. M., Cimatti A., Daddi E., Pozzetti L., Vanzil L., 2001, *MNRAS*, 326, 745
- Martin C. L., Shapley A. E., Coil A. L., Kornei K. A., Bundy K., Weiner B. J., Noeske K. G., Schiminovich D., 2012, *arXiv*, arXiv:1206.5552
- Ménard B., Chelouche D., 2009, *MNRAS*, 393, 808
- Ménard B., Wild V., Nestor D., Quider A., Zibetti S., Rao S., Turnshek D., 2011, *MNRAS*, 417, 801
- More S., van den Bosch F. C., Cacciato M., Skibba R., Mo H. J., Yang X., 2011, *MNRAS*, 410, 210
- Nestor D. B., Turnshek D. A., Rao S. M., 2005, *ApJ*, 628, 637
- Nestor D. B., Johnson B. D., Wild V., Ménard B., Turnshek D. A., Rao S., Pettini M., 2011, *MNRAS*, 412, 1559
- Petitjean P., Bergeron J., 1990, *A&A*, 231, 309
- Prochaska J. X., Hennawi J. F., 2009, *ApJ*, 690, 1558
- Prochter G. E., Prochaska J. X., Burles S. M., 2006, *ApJ*, 639, 766
- Quashnock J. M., vanden Berk D. E., 1998, *ApJ*, 500, 28
- Quashnock J. M., Stein M. L., 1999, *ApJ*, 515, 506
- Rao S. M., Turnshek D. A., Nestor D. B., 2006, *ApJ*, 636, 610
- Richards G. T., et al., 2006, *ApJS*, 166, 470
- Rigby J. R., Charlton J. C., Churchill C. W., 2002, *ApJ*, 565, 743
- Rubin K. H. R., Prochaska J. X., Koo D. C., Phillips A. C., 2012, *ApJ*, 747, L26
- Rubin K. H. R., Prochaska J. X., Koo D. C., Phillips A. C., Weiner B. J., 2010, *ApJ*, 712, 574
- Sancisi R., Fraternali F., Oosterloo T., van der Hulst T., 2008, *A&ARv*, 15, 189
- Sanmartim D., Storchi-Bergmann T., Brotherton M. S., 2012, *arXiv*, arXiv:1210.1208
- Sbarufatti B., Treves A., Falomo R., Heidt J., Kotilainen J., Scarpa R., 2005, *AJ*, 129, 559
- Scargle J. D., Caroff L. J., Noerdlinger P. D., 1970, *ApJ*, 161, L115
- Schneider D. P., et al., 1993, *ApJS*, 87, 45
- Schneider D. P., et al., 2010, *AJ*, 139, 2360
- Schlegel D. J., Finkbeiner D. P., Davis M., 1998, *ApJ*, 500, 525
- Schirber M., Miralda-Escudé J., McDonald P., 2004, *ApJ*, 610, 105
- Serber W., Bahcall N., Ménard B., Richards G., 2006, *ApJ*, 643, 68
- Shaver P. A., Boksenberg A., Robertson J. G., 1982, *ApJ*, 261, L7
- Shaver P. A., Robertson J. G., 1983, *ApJ*, 268, L57
- Shaver P. A., Robertson J. G., 1985, *MNRAS*, 212, 15P
- Shen Y., et al., 2011, *ApJS*, 194, 45
- Shen Y., Ménard B., 2011, *arXiv*, arXiv:1104.0778
- Srianand R., Khare P., 1993, *ApJ*, 413, 486
- Srianand R., Khare P., 1994, *ApJ*, 428, 82
- Steidel C. C., Dickinson M., Persson S. E., 1994, *ApJ*, 437, L75
- Steidel C. C., Sargent W. L. W., 1992, *ApJS*, 80, 1
- Sulentic J. W., Rosado M., Dultzin-Hacyan D., Verdes-Montenegro L., Trinchieri G., Xu C., Pietsch W., 2001, *AJ*, 122, 2993
- Tinker J. L., Chen H.-W., 2008, *ApJ*, 679, 1218
- Turnshek D. A., 1984, *ApJ*, 280, 51
- Tremonti C. A., Moustakas J., Diamond-Stanic A. M., 2007, *ApJ*, 663, L77
- Tripp T. M., Bowen D. V., 2005, *pgqa.conf*, 5
- Tytler D., Fan X.-M., 1992, *ApJS*, 79, 1
- Tytler D., et al., 2009, *MNRAS*, 392, 1539
- Weiner B. J., et al., 2009, *ApJ*, 692, 187

- Wild V., et al., 2008, MNRAS, 388, 227
Wold M., Lacy M., Lilje P. B., Serjeant S., 2001, MNRAS, 323, 231
Worseck G., Wisotzki L., 2006, A&A, 450, 495
Vanden Berk D., et al., 2008, ApJ, 679, 239
Vestergaard M., Wilkes B. J., 2001, ApJS, 134, 1
Vestergaard M., 2003, ApJ, 599, 116
Vestergaard M., Peterson B. M., 2006, ApJ, 641, 689
Vestergaard M., Osmer P. S., 2009, ApJ, 699, 800
Véron-Cetty M.-P., Véron P., 2010, A&A, 518, A10
Young P., Sargent W. L. W., Boksenberg A., 1982, ApJS, 48, 455
Zwaan M. A., van der Hulst J. M., Briggs F. H., Verheijen M. A. W., Ryan-Weber E. V., 2005, MNRAS, 364, 1467
Zibetti S., Ménard B., Nestor D. B., Quider A. M., Rao S. M., Turnshek D. A., 2007, ApJ, 658, 161

APPENDIX A: NOTES ON INDIVIDUAL OBJECTS

QQ01 — The Mg II absorption lines in QQ01B is detected at a level slightly lower than the considered 3σ threshold. However, since the large uncertainties in the continuum location, we have maintained this absorption system in the analysis.

QQ04 — The two QSOs of the pair are very close in redshift thus the association of the absorption feature to the foreground or to the background QSO is uncertain. QQ04F shows two CIV absorption systems superimposed to the broad emission line. A stronger one at redshift $z_{\text{abs}} \sim 2.1120$ and a fainter blueshifted one at $z_{\text{abs}} \sim 2.1350$. The two component of the stronger absorption system are partially blended, and thus fitted simultaneously with the sum of two Gauss functions. Moreover, other absorptions lines are present at $\lambda = 4822.7 \text{ \AA}$ and at $\lambda = 4845.8 \text{ \AA}$, whose identification is uncertain as they are superimposed on the stronger absorption system.

Due to the velocity range that we have considered to associate the absorption features to the QSO_F (see §4), we have assumed that the stronger feature is due to the QSO halo, while the weaker one (with $\Delta V \sim 3000 \text{ km/s}$ from the former) to a simple chance superposition. However, the uncertainties in the redshift determination based on CIV broad emission line are large, mostly due to the presence of the strong absorption features (see e.g., Hewett & Wild 2010). This does not allow to exclude the possibility that the weaker absorption system is connected to the QSO_F halo and that the stronger one is due to a gas outflow. QQ04B shows a broad absorption lines in the blue wing of the CIV emission lines. These P-Cygni like profile, are usually interpreted as radiatively driven winds associated to strong outflows from QSOs (e.g., Scargle, Caroff, & Noerdlinger 1970; Turnshek 1984). In the spectra of QQ04B, two more CIV absorption features are present at redshift $z_{\text{abs}} = 2.0302$ and $z_{\text{abs}} = 2.0443$, suggesting a very rich environment for this pair or an interaction between the QSOs (see Table A1).

QSO05 — In the spectra of QQ05B we detect Fe II($\lambda 2586$) and Fe II($\lambda 2600$) lines at the same redshift of the Mg II doublet associated to the QSO_F ($EW_{\text{r}}(\lambda 2586) = (0.12 \pm 0.04) \text{ \AA}$ and $EW_{\text{r}}(\lambda 2600) = (0.39 \pm 0.04) \text{ \AA}$).

QSO07 — Associated to the Mg II absorption feature at

redshift $z_{\text{abs}} = 1.3355$ (see Table A1) we detect Fe II($\lambda 2586$) and Fe II($\lambda 2600$) lines with $EW_{\text{r}}(\lambda 2586) = (0.61 \pm 0.07) \text{ \AA}$ and $EW_{\text{r}}(\lambda 2600) = (0.70 \pm 0.04) \text{ \AA}$. A Fe II($\lambda 2382$) line is present at the same redshift of the Mg II doublet at $z_{\text{abs}} = 1.5186$ ($EW_{\text{r}}(\lambda 2382) = (0.23 \pm 0.04) \text{ \AA}$).

QSO10 — Two CIV doublets are superimposed to the CIV broad emission of QSO_B. Their redshifts are $z_{\text{abs}} = 2.5127$ and $z_{\text{abs}} = 2.5167$, corresponding to a velocity difference of $\sim 500 \text{ km/s}$ (see Table A1). Due to the large uncertainties in the QSO redshift determination from broad emission lines (see §4), both the systems could be associated to the QSO.

QSO13 — This pair was already investigated by Decarli, Treves, & Falomo (2009), which have noticed a non resolved Mg II absorption feature associated to the foreground QSO. Moreover they observe QSO13F in Ks band to detect the host galaxy. This allows to give a independent estimate of the host galaxy mass ($M_{\text{host}} = 5 \times 10^{11} M_{\odot}$) that is consistent with the value estimated indirectly from the M_{BH} .

In the spectra of QSO_B we identify two CIV doublet at redshifts discordant with that of the QSO ($z_{\text{abs}} \sim 2.3215$ and $z_{\text{abs}} \sim 2.3272$). Due to their redshift difference the component of the doublets are superimposed, we thus infer the EW_{r} assuming that the lines are not saturated and thus a theoretical doublet ratio value of $DR = 2$ (see Table A1).

Table A1. Properties of Mg II and C IV absorption features not associated to QSO_F detected on the QSO spectra: our identification label of the QSO (ID), feature detected (Abs.), observed wavelength (λ_{abs}), rest frame equivalent width (EW_r), doublet ratio (DR), and redshift (z_{abs}).

Mg II						
ID	$\lambda_{\text{abs}}(\lambda 2796)$ [Å]	$\text{EW}_r(\lambda 2796)$ [Å]	$\lambda_{\text{abs}}(\lambda 2803)$ [Å]	$\text{EW}_r(\lambda 2803)$ [Å]	DR	z_{abs}
QQ01F	5954.7	0.86±0.15	5970.3	0.45±0.14	1.91±0.68	1.1294±0.0001
QQ07B	6378.1	0.46±0.06	6395.0	0.43±0.03	1.07±0.16	1.2810±0.0002
QQ07B	6531.0	1.10±0.04	6547.9	1.09±0.06	1.01±0.07	1.3355±0.0001
QQ07B	7042.9	0.58±0.06	7061.0	0.46±0.04	1.26±0.17	1.5186±0.0002
QQ08B	6958.9	1.02±0.10	6975.6	0.51±0.11	2.00±0.47	1.4882±0.0008
C IV						
ID	$\lambda_{\text{abs}}(\lambda 1548)$ [Å]	$\text{EW}_r(\lambda 1548)$ [Å]	$\lambda_{\text{abs}}(\lambda 1551)$ [Å]	$\text{EW}_r(\lambda 1551)$ [Å]	DR	z_{abs}
QQ04B	4691.5	0.54±0.03	4699.1	0.37±0.02	1.46±0.11	2.0302±0.0002
QQ04B	4713.4	0.27±0.02	4721.0	0.22±0.05	1.23±0.29	2.0443±0.0003
QQ10B	5438.4	0.22±0.03	5447.4	0.16±0.06	1.38±0.55	2.5127±0.0002
QQ10B	5444.7	0.19±0.06	5453.6	0.19±0.04	1.00±0.38	2.5167±0.0002
QQ13B	5142.3	0.14±0.03	5151.1	0.07±0.03	2.00±0.96 [†]	2.3215±0.0001
QQ13B	5151.1	0.40±0.03	5159.7	0.20±0.03	2.00±0.34 [†]	2.3272±0.0001

[†] Assumed value for DR (see text for details)